Energy 227 (2021) 120396

Contents lists available at ScienceDirect

Energy

journal homepage: www.elsevier.com/locate/energy

Compound-choking theory for supersonic ejectors working with real gas

Sergio Croquer [a,*], Yu Fang [a,b], Antoine Metsue [a,b], Yann Bartosiewicz [b], Sébastien Poncet [a]

[a] Département de Génie Mécanique, Université de Sherbrooke, 2500 Boulevard de L'Université, Sherbrooke, QC, J1K 2R1, Canada
[b] Université Catholique de Louvain (UCLouvain), Institute Mechanics, Materials, and Civil Engineering (iMMC), Louvain-la-Neuve, 1348, Belgium

A R T I C L E I N F O

Article history:
Received 26 November 2020
Received in revised form
17 February 2021
Accepted 14 March 2021
Available online 29 March 2021

Keywords:
Supersonic ejector
Real gas
Compound-choking
Fabri-choking
CFD
Thermodynamic modeling

A B S T R A C T

The performance of supersonic ejectors is mainly limited by the choking of the flow. Below a critical pressure, the entrainment capability of the ejector remains indeed constant. As the coefficient of performance of ejector-based heat driven refrigeration cycles (HDRC) is directly linked to the ejector entrainment ratio, it constitutes a real limitation towards better overall cycle performance. The compound-choking criterion has recently demonstrated to better explain this limitation compared to the Fabri-choking theory for supersonic ejectors working with air. However, as all ejector-driven HDRCs work with real gas refrigerants, this criterion needs to be extended to real gases. In the present work, the compound-choking criterion is first extended analytically to real gases. Wall-resolved turbulence modelings for supersonic ejectors working with R134a and blends of R134a and HydroFluoroOlefeins (HFO) are then performed. An improved thermodynamic model is finally used to demonstrate the superiority of the compound-choking criterion over the Fabri-choking one for supersonic ejectors. Results show that the β parameter constitutes an unambiguous indicator of the ejector choking condition, much better suited to determine the operating regime than the sonic line criterion. Moreover, the mean error in entrainment ratio predictions is reduced from 17.54% to 5.28% when using the compound-choking theory instead of the Fabri-choking one, with virtually no difference in the complexity or computational cost of the model.

1. Introduction

Single-phase ejectors are the subject of renewed interest in the refrigeration industry as they may be used to assist or replace the compressor in a conventional vapor compression cycle, but with some sacrifice in the coefficient of performance (COP) of the system. In particular, their application in heat driven refrigeration cycles (HDRC) appeared as a very promising technology since they may be thermally activated by waste heat or low-grade energy from renewable sources. Supersonic ejectors being relatively simple devices with no moving parts and no maintenance costs, their low inherent efficiencies do not represent a major concern for their widespread application. The interested reader can refer to the recent review paper of Aidoun et *al*. [1] or the reference monograph of Grazzini et *al*. [2] for more details about the applications of single-phase ejectors in the refrigeration industry and recent achievements in ejectors.

A supersonic ejector may be seen as a convergent-divergent nozzle for the primary stream embedded in a larger one. The primary stream reaches supersonic conditions at the end of the divergent part. This high speed flow sucks the secondary stream. Both streams starts mixing at the beginning of the constant section area (CSA). A series of oblique shock waves appears in the CSA or at the beginning of the diffuser. After this shock-train, the mixed stream is compressed to reach the outlet pressure fixed by the condenser in a HDRC. The performances of single-phase supersonic ejectors are usually quantified by two global parameters, namely the entrainment ratio $\omega = \dot{m}_s/\dot{m}_p$ and the compression ratio $\Gamma = p_{out}/p_{s,0}$, where $\dot{m}_p$ and $\dot{m}_s$ denote the mass flowrates of the primary and secondary streams, p_{out} is the outlet or back pressure and $p_{s,0}$ the secondary inlet pressure. According to the variations of ω with p_{out}, one may distinguish three distinct regimes (clearly shown on the operating curve of Fig. 5(a) for example):

* Corresponding author.
E-mail address: sergio.croquer@usherbrooke.ca (S. Croquer).

https://doi.org/10.1016/j.energy.2021.120396
0360-5442/

- the double-choking (or on-design) regime for $p_{out} < p_{lim}$, where p_{lim} is the critical or limiting outlet pressure. The entrainment ratio is then constant irregardless of the back pressure.
- $p_{out} = p_{lim}$ represents the critical point, for which an ejector is designed.
- the single-choking (or off-design) regime for $p_{out} > p_{lim}$. The entrainment ratio ω is then a decreasing function of p_{out}. Beyond a certain critical value of p_{out} (for which $\omega = 0$), the ejector starts malfunctioning, which means that a further increase of the back pressure may cause backflow to appear at the secondary inlet. The primary stream remains choked in the primary nozzle.

The choking phenomenon is crucial in supersonic ejectors as it is responsible for the plateau on the (ω, p_{out}) operating curve. As, in an ejector-based HDRC, the COP of the system is directly proportional to the entrainment ratio ω of the ejector, the choking of the flow may drastically limit their performance [3]. It is then of prime importance to better understand this phenomenon to both predict it accurately and maximize it for an appropriate system design. Most of the simplified thermodynamic models published so far in the literature are based on the Fabri-choking theory, a few examples of models based on this theory can be found in Refs. [4–10]. Named after the pioneering work of Fabri and Siestrunck [11], this theory emerged from wall pressure measurements and flow visualizations in a rectangular ejector working with air. The authors assumed that the secondary flow reaches sonic conditions at a given distance from the primary nozzle outlet in a hypothetical throat (or effective area) due to the pinching of the secondary stream between the ejector wall and the primary stream jet. The main limitation of this theory is that the existence of the Fabri-choking has been experimentally reported only once in the literature by Lamberts et al. [12]. The authors performed Schlieren visualizations and wall-resolved turbulence modelings of a rectangular ejector working with air. They observed a characteristic Fabri-choking pattern (Y-shocks in the secondary stream) for very specific conditions and only in a narrow range of $0.343 \leq p_{out}/p_{p,0} \leq 0.394$ ($p_{p,0}$ being the inlet primary pressure); furthermore they did not observe, neither experimentally nor numerically, this signature for other conditions while the ejector was actually choked. Although the Fabri-choking has been confirmed experimentally and by numerical simulations, its lack of generality for other refrigerants and operating conditions may partly explain why such thermodynamic models fail to predict accurately the entrainment ratio for the on-design regime. Just as an example, Garcia del Valle et al. [6] reported deviations up to 17%, which is typical of such models as it will be shown here in Section 3.2. Another theory, the compound-choking, exists to explain the entrainment limitation in supersonic ejectors. The term has been first introduced by Bernstein et al. [13]. Their theory consists in a one-dimensional compound-compressible theory for the flow of gas streams in a single nozzle. Their results confirmed the former work of Pearson et al. [14], who developed, based on a wave velocity argument, a choked flow condition for two perfect gases at different states flowing in a cylindrical ejector. Lamberts et al. [15] performed simulations using a wall-resolved k-ω SST model for a rectangular ejector working with air. After a careful model validation against their own experimental data (see in Refs. [12,15]), they used their numerical and experimental results to discuss in details the performance of the compound-choking theory to predict the entrainment ratio in the on-design regime for different sets of operating conditions. The authors concluded that this theory is more suited to physically explain and then to model the choking process in supersonic ejectors compared to the Fabri-choking theory. The interested reader can refer to the works of Lamberts et *al.* [12,15] for a more detailed discussion about the Fabri- and compound-choking theories applied to supersonic ejectors. The main objective of the present paper is to extend the former work of Lamberts et *al.* [15] to real gas supersonic ejectors. To the best of the authors' knowledge, a compound-choking criterion has never been proposed in the open literature for real gas flows neither in convergent-divergent nozzles nor in supersonic ejectors. This new criterion developed analytically will be then discussed regarding new results obtained both by a wall-resolved k-ω SST model and by an improved version of the Chen et *al.*'s [8] thermodynamic model including this choking model. The paper is organized as follows. The compound-choking criterion is first extended analytically to real gases in Section 2. Section 3.1 proposes comparisons between the sonic line and compound-choking criteria obtained by a 2D axisymetric k- ω SST model for real gases including here R134a and blends of R134a and hydrofluorooleifins (HFO). The discussion is further substantiated in Section 3.2, where the compound-choking criterion is verified by using an improved version of the Chen et *al.*'s [8] thermodynamic model. It ends with a summary of the main results and future works in Section 5.

2. Compound-chocking theory for real gases

The compound-compressible flow theory was first proposed by Bernstein et *al.* [13] to analyze the choking conditions of parallel gas streams in a converging-diverging nozzle. A schematic of the compound-compressible nozzle flow is shown in Fig. 1.

The flow through the nozzle is divided into several parallel substreams with individual stagnation conditions and thermodynamic properties. The compound-choking theory states that for fixed inlet conditions and reducing the outlet pressure, there is a point where information (defined by a compound wave) cannot propagate upstream even if some of the individual streams are still subsonic, i.e., the flow is compound-choked. The main assumptions of the original compound-choking theory are:

- The flow is one-dimensional, steady, adiabatic and isentropic.
- Each flow stream is a perfect gas with constant thermodynamic properties.
- There is no mixing between streams.
- The static pressure is constant across all streams and only varies in the streamwise direction.

2.1. Compound-flow indicator for real gases

In comparison with the classical single-gas theory, which determines the choking condition according to the local Mach number, the compound-choking theory defines a compound-flow indicator β as the choking criterion [13]:

$$\beta = \sum_{i=1}^{n} \frac{A_i}{\gamma_i} \left(\frac{1}{M_i^2} - 1 \right), \tag{1}$$

where A_i, γ_i and M_i denote the cross-sectional area, heat capacity ratio, and Mach number of each stream, respectively. The subscript "i" represents the individual sub-streams. Then, the flow regimes are divided as follows:

- $\beta > 0$: compound-subsonic flow.
- $\beta = 0$: compound-sonic flow.
- $\beta < 0$: compound-supersonic flow.

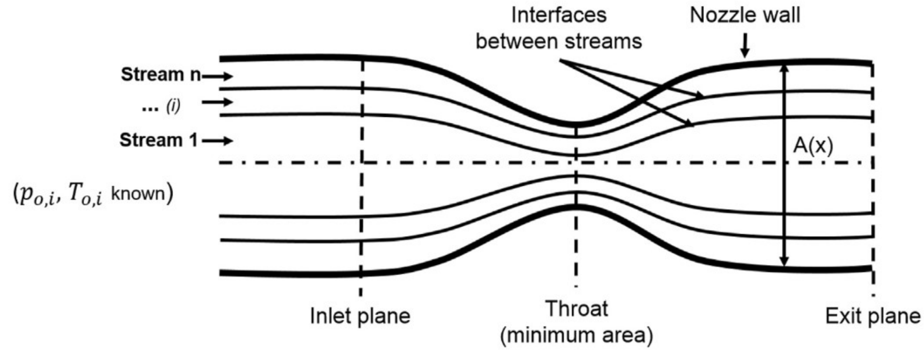

Fig. 1. Schematic of the compound-compressible nozzle flow. Adapted from Ref. [13].

In this study, the compound-choking theory is extended to real gas flows. Hence, the perfect gas parts are adapted for real gas refrigerants. The equations for the conservation of mass and momentum of each stream can be written as:

$$\rho_i V_i A_i = constant \Rightarrow \frac{d\rho_i}{\rho_i} + \frac{dV_i}{V_i} + \frac{dA_i}{A_i} = 0 \tag{2}$$

$$\rho_i V_i A_i dV_i = -A_i dp_i \tag{3}$$

From Equation (2), one gets:

$$dV_i = -V_i\left(\frac{d\rho_i}{\rho_i} + \frac{dA_i}{A_i}\right) \tag{4}$$

Then, substituting dV_i in Equation (3) by Equation (4) and $d\rho_i$ by $d\rho = \left(\frac{\partial\rho}{\partial p}\right)_s dp$, one gets the following equation by introducing the speed of sound (appearing in the Mach number):

$$\frac{dA_i}{A_i} = \frac{dp_i}{\rho_i V_i^2}\left(1 - M_i^2\right) \tag{5}$$

According to the assumptions previously made, the cross-sectional pressure is constant for each stream, so one can write $dp_i = dp$. Finally, the compound-choking indicator can be rewritten as:

$$\beta = p\sum_i \frac{A_i}{\rho_i V_i^2}\left(1 - M_i^2\right) \tag{6}$$

One can then easily verify that for a perfect gas: $\frac{p}{\rho_i V_i^2} = \frac{Rg_i T_i}{V_i^2} = \frac{c_i^2}{\gamma_i V_i^2} = \frac{1}{\gamma_i M_i^2}$, when it is introduced in Eq. (6), it results in the original formulation of Bernstein et *al*. [13] (Eq. (1)).

2.2. Analysis in the moving frame of a compound wave

The behavior of β for real gases in the compound wave frame has to be verified. One considers an individual sub-stream i submitted to a cross-section change. Its pressure is p_i in the section A_i and $p_i + dp_i$ in the section $A_i + dA_i$, where dA_i and dp_i are the cross-section and pressure variations between two successive points. One also arbitrarily defines a compound wave moving upstream with speed α. If the absolute flow velocity is V_i, the flow velocity in the frame of the compound wave is:

$$V_i' = V_i + \alpha \tag{7}$$

where the upstream propagating direction of the compound wave is directly given by its sign: $\alpha > 0$ corresponds to a compound-subsonic flow; $\alpha = 0$ corresponds to a compound-sonic flow; $\alpha < 0$ corresponds to a compound-supersonic flow. In the frame of the compound wave, the mass and momentum conservation equations write:

$$\rho_i V_i' A_i = (\rho_i + d\rho_i)(V_i' + dV_i')(A_i + dA_i) = cst \tag{8}$$

$$p_i A_i - (p_i + dp_i)(A_i + dA_i) + p_i dA_i = \rho_i V_i' A_i (V_i' + dV_i' - V_i') \tag{9}$$

Then, the previous equations become:

$$\frac{d\rho_i}{\rho_i} + \frac{dV_i}{V_i'} + \frac{dA_i}{A_i} = 0 \tag{10}$$

where $dV_i = dV_i'$, and

$$\frac{dp_i}{p_i} + \frac{\rho_i V_i'^2}{p_i}\frac{dV_i}{V_i'} = 0 \tag{11}$$

The local speed of sound for the stream i is defined by $c_i^2 = \left(\frac{\partial p_i}{\partial \rho_i}\right)_s$, or can be also written:

$$\frac{d\rho_i}{\rho_i} = \frac{1}{c_i^2}\frac{dp_i}{\rho_i} \tag{12}$$

After introducing Equation (12) into Equation (10), one gets:

$$\frac{1}{c_i^2}\frac{dp_i}{\rho_i} + \frac{dV_i}{V_i'} + \frac{dA_i}{A_i} = 0 \Rightarrow \frac{dV_i}{V_i'} = -\left(\frac{dA_i}{A_i} + \frac{1}{c_i^2}\frac{dp_i}{\rho_i}\right) \tag{13}$$

After substituting $\frac{dV_i}{V_i'}$ in Equation (11) by Equation (13), one obtains:

$$\frac{dA_i}{A_i} = \frac{dp_i}{\rho_i}\left(\frac{1}{V_i'^2} - \frac{1}{c^2}\right) \tag{14}$$

Moreover, V_i' is replaced by using Equation (7) and $p = p_i$ still holds. Thus:

$$\frac{dA_i}{A_i} = \frac{dp}{\rho_i}\left[\frac{1}{(\alpha + M_i c_i)^2} - \frac{1}{c_i^2}\right] \tag{15}$$

Since the compound wave is assumed to be very thin, the variations between two successive cross-sectional areas are negligible. Thus, one can write:

$$\sum dA_i = 0 \Rightarrow \sum \frac{A_i}{\rho_i V_i^2} M_i^2 = \sum \frac{A_i}{\rho_i V_i^2} \frac{1}{\left(\frac{\alpha}{V_i} + 1\right)^2} \tag{16}$$

Finally, by introducing Eq. (16) into Eq. (6), β can be rewritten based on the compound wave propagating speed as:

$$\beta = p \sum_i \frac{A_i}{\rho_i V_i^2} \left[1 - \frac{1}{\left(\frac{\alpha}{V_i} + 1\right)^2} \right] \tag{17}$$

This relation verifies the flow regimes by α and β, which are summarized as:

- $\alpha > 0$: compound-subsonic flow $\rightarrow \beta > 0$.
- $\alpha = 0$: compound-sonic flow $\rightarrow \beta = 0$.
- $\alpha < 0$: compound-supersonic flow $\rightarrow \beta < 0$.

Hence, the choking criterion based on the compound-compressible flow theory for real gases,

$$\beta = p \sum_i \frac{A_i}{\rho_i V_i^2} \left(1 - M_i^2\right) = 0 \tag{18}$$

is the proper criterion representing the relative celerity of a pressure wave propagating in the compound-flow, and hence characterizing its potential choked condition.

In the following sections, one will apply the extended compound-compressible flow theory to better understand the choking phenomenon and the entrainment ratio limitation in supersonic ejectors working with real gas refrigerants. As shown in Fig. 2, the flow through the ejector is conformed by two streams, which can be separated (in average) by a dividing stream line. By construction, mass is conserved in each sub-stream and there is no flow across the dividing streamline. One can compute the compound-choking indicator β (Eq. (6)) based on these two sub-streams to determine the choking conditions. As a result, the choking location where β is equal to zero can be found and at this location the secondary stream can be still subsonic while the primary stream is supersonic.

3. Methods

Two numerical approaches have been developed. Firstly, a RANS model is used to study the applicability of the compound choke theory on the internal flow of the ejector. This model has already been presented and thoroughly validated in previous studies on ejectors [16]. Secondly, a thermodynamic model based on the work of [8] but using the compound flow theory as choking condition has been developed to assess the use of this theory for the prediction of ejector entrainment ratio.

3.1. RANS modeling

3.1.1. Ejector geometry and operating conditions

The ejector geometry and operating conditions are based on the experimental work of Garcia del Valle et *al.* [17] on a supersonic ejector developed for a heat-driven refrigeration cycle working with R134a. A schematic view of the ejector is displayed in Fig. 2 with the main relevant notations. Its main dimensions are summarized in Table 1. Additional to R134a, this numerical study also considers two mixtures of R134a-R1234yf and R134a-R1234ze(E) as working fluids. R1234yf and R1234ze(E) are synthetic HFO fluids designed to substitute typical hydrofluorocarbon (HFC) refrigerants such as R134a and R245fa. As seen in Table 2, these HFO fluids have zero ozone depletion potential and negligible global warming potential but higher flammability than R134a. For these reasons, mixtures of R134a-R1234ya and R134a-R1234ze(E) are recognized as viable drop-in replacements of R134a, which combine the low environmental impact of HFOs with the higher performance and lower flammability of R134a [18]. In particular, R134a-R1234yf mixtures have shown promising applicability in the refrigeration industry [19], whereas vapor-compression systems using blends of R134a and R1234ze(E) have shown larger operating ranges and a COP increase of about 1.5% depending on the operating conditions [20]. Table 3 summarizes the combination of working fluids and operating conditions studied using the RANS model. Operating points OP1 and OP2 refer to the combination of pressure and temperature conditions for each case. These include a 10 °C overheat at the inlets to ensure that the refrigerant remains gaseous throughout the whole ejector.

3.1.2. Numerical setup

The computational model used in this investigation combines the solution of the RANS equations with the $k-\omega$ SST model in its low-Reynolds formulation and the REFPROP 7.0 database for

Table 1
Main dimensions of the ejector.

Parameter	Value [mm]
Primary nozzle throat diameter, n_d	2.00
Primary nozzle exit diameter, d	3.00
Nozzle Exit Position, *NXP*	− 5.38
Mixing chamber diameter, D	4.80
Mixing chamber length, l	41.39
Diffuser length, L	120.15
Outlet diameter, e_d	20

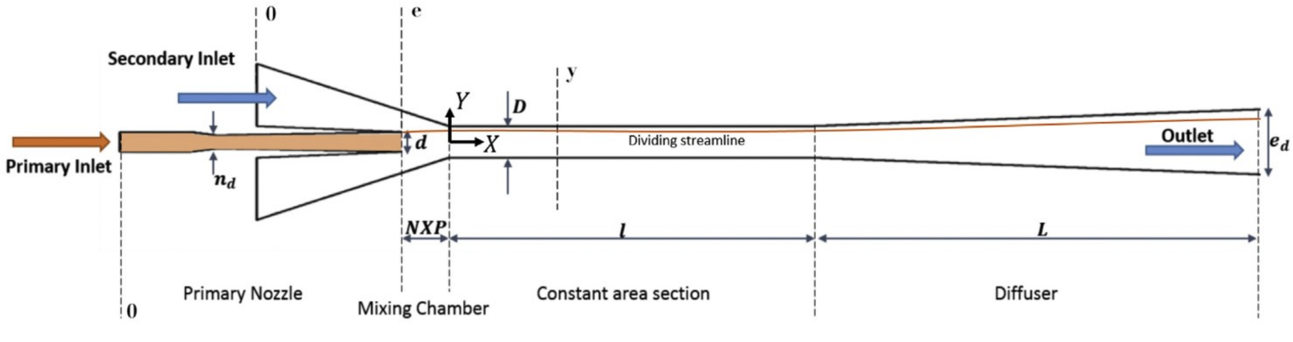

Fig. 2. Schematic of the ejector along with the definition of the main geometrical parameters.

Table 2
Thermodynamic properties of R134a, R1234yf and R1234ze(E). GWP_{100} is the Global Warming Potential over a 100 year integration horizon.

Working Fluid	*R134a*	*R1234yf*	*R1234ze(E)*
Name	1,1,1,2 tetrafluoroethane	2,3,3,3 tetrafluoroprop-1-ene	1,3,3,3 tetrafluoroprop-1-ene
Chemical formula	CF_3CFH_2	$CH_2 = CFCF_3$	$CF_3CH = CHF$
Molecular weight ($g.mol^{-1}$)	102.03	114.04	114.04
Toxicity class (Ashrae Std 34)	A (low)	A (low)	A (low)
Flammability (Ashrae Std 34)	A1 (non flammable)	A2L (low flammability)	A2L (low flammability)
GWP_{100}	1430	4	4
Ozone Depletion Potential (ODP)	0	0	0
Lifetime in the atmosphere (year)	13	0.03	0.05
Normal boiling point ($^{\circ}C$)	− 26.1	− 29.4	− 18.95
Saturated vapor pressure at 20$^{\circ}C$ (kPa)	774.3	794.3	419.2
Saturated vapor pressure at 80$^{\circ}C$ (kPa)	2635	2519	2007
Critical temperature ($^{\circ}C$)	101.1	94.7	109.4
Critical pressure (MPa)	4.059	3.38	3.635
Density ($kg.m^{-3}$) at 30$^{\circ}C$			
Liquid phase	1187	1075	1146
Vapor phase	37.54	44	30.6
Heat capacity C_p ($kJ.kg^{-1}.K^{-1}$) at 30$^{\circ}C$			
Liquid phase	1.446	1.379	1.383
Vapor phase	1.065	1.11	0.9822
Thermal conductivity k ($W.m^{-1}.K^{-1}$) at 30$^{\circ}C$			
Liquid phase	0.079	0.0631	0.0725
Vapor phase	0.01433	0.01143	0.014
Dynamic viscosity μ ($\mu Pa.s^{-1}$) at 30$^{\circ}C$			
Liquid phase	185.8	152	188
Vapor phase	12.04	12.86	12.5
Latent heat of vaporization at 30$^{\circ}C$ ($kJ.kg^{-1}$)	173.1	140.1	162.9

Table 3
Summary of the 5 cases assessed in this work.

Working fluid	Operating point	$T_{p,0}$ [°C]	$T_{s,0}$ [°C]	$p_{p,0}$ [kPa]	$p_{s,0}$ [kPa]	ω [−]	p_{lim} [kPa]
R134a	OP1	89.35	20.05	2598.0	414.6	0.513	787.2
R134a	OP2	94.35	20.05	2888.8	414.6	0.436	862.6
20%R134a-80%R1234yf	OP1	89.35	20.05	2598.0	414.6	0.496	797.2
20%R134a-80%R1234ze(E)	OP1	89.35	20.05	2598.0	414.6	0.408	857.2
80%R134a-20%R1234yf	OP2	94.35	20.05	2888.8	414.6	0.433	857.2

calculating the fluid properties. This setup has been determined via a benchmark study on the same ejector and operating conditions presented in Ref. [16]. The benchmark assessed several choices of turbulence model, near-wall treatment formulation, gas properties equations method and mesh independence analysis. The configuration offering the best compromise between accuracy and computational cost has been then used in this investigation. For the sake of brevity, a brief description of the model is provided here.

The system of conservation equations is solved using a finite-volume approach in *ANSYS Fluent v.18* on a 2D axisymmetric computational domain as shown in Fig. 2. The k-ω SST turbulence model is used to close the system of RANS equations. Associated to an appropriate mesh grid, this model is directly useable all the way down to the wall (wall-resolved model). This approach has shown better performance over other two-equation turbulence models when dealing with gas supersonic ejectors [16,21].

Second-order upwind and second-order central difference discretization schemes are applied to the advective and diffusive terms, respectively. A least-squares technique is used to approximate the gradient terms. A pressured-based algorithm is adopted to overcome the pressure-velocity coupling. This approach has been successfully applied in supersonic ejectors in former studies [16,22,23]. Fluid properties are calculated using the NIST REFPROP Database [24], which provides calibrated equations of state for several refrigerants and mixtures.

In terms of boundary conditions, total pressure and total temperature are prescribed at both inlets whereas static pressure is fixed at the outlet according to the operating points of Table 3. For fluid mixtures, the corresponding R134a mass fraction is also fixed at both inlets. This mass fraction is constant and uniform through the ejector, i.e., there is no species separation. Walls are considered as smooth and adiabatic.

Following a mesh convergence study, the domain is discretized using a grid of 650,000 structured elements. The resulting mesh is refined in the mixing layer and the constant area section. Moreover, 21 prismatic layers are also imposed close to the walls to guarantee $y^+ \leq 1$ at walls.

A series of python scripts were used to extract the dividing streamline coordinates, $M = 1$ and β profiles through the ejector using the c, V, p and ρ fields. The RANS figures were produced using the postprocessing tool *Paraview v.5.5.2* [25]. No User Defined Functions were deemed necessary.

A thorough experimental validation of this numerical setup has already been performed in former studies, both in terms of the entrainment and pressure ratios [16] and of the pressure profile through the device [26]. In summary, for the cases with pure R134a in Table 3, the model provides results with a deviation of up to 5% in terms of ω and of up to 0.5% in terms of p_{lim} relative to the experimental data of [17]. Although validation has been carried out only for R134a, similar deviations are expected in the cases of R1234yf and R1234ze(E) given the very similar properties between these three gases. The interested reader can refer to the former paper of Croquer et *al.* [16] for more details about the numerical set-up.

3.2. Thermodynamic modeling

In this section, one proposes to compare the classical (Fabri-) choking criterion to the compound-choking criterion for critical operating conditions by using a thermodynamic model implemented in Python. Both models (Fabri and compound) only differ in their choking conditions, and are based on the model of Chen et *al.* [8]. In fact, the thermodynamic model that will be used to compute the performance of the Fabri-choking criterion is in all ways similar to the one of Chen et *al.* [8]. The differences between the compound-choking model and the model of Chen et *al.* [8] will be discussed hereafter. As a reminder, the main assumptions for the present models (both Fabri- and compound-choking) are:

1. The flow is one dimensional, steady and adiabatic. The inlets (primary and secondary), as well as the outlet velocities, are negligible [1].
2. For the sake of simplicity, the transformations are here assumed to be isentropic, although friction losses can be taken into account with the use of multiple isentropic efficiencies [1].
3. Real gas properties will be retrieved from the tabulated data provided by the COOLPROP library [27], which is a free access alternative to the NIST REFPROP Database [24] and uses the same equations of state for the assessed gases.
4. Primary and secondary flows do not start mixing up until the so-called mixing section (section y in Fig. 2) located inside of the constant area duct [7].
5. The pressure is uniform at each crossed section.

Let us first introduce the Fabri-choking criterion. Using said criterion comes down to maximizing primary and secondary flows separately. More precisely, the primary flow is maximized, and the secondary flow is expanded until reaching the maximum mass flow per unit area ($G\,[kg.m^{-2}.s^{-1}]$). Building on the hypothesis that both streams have the same pressure at the location of the hypothetical throat, the primary flow is then further expanded, from the primary nozzle exit up until reaching the secondary pressure at the maximum mass flow per unit area. This choking criterion, despite being the most widely used in the literature, does not take into account the fact that the maximum mass flow through an ejector does not automatically happen when the secondary flow reaches sonic conditions, but rather when the secondary flow is still subsonic. The compound-choking criterion allows such configuration, which usually translates in higher values of the entrainment ratio compared to the Fabri-choking. Note that this is not necessarily true when friction is accounted for, since the coumpound-choking indicator ($\beta = 0$) assumes that the transformations are isentropic. This actually means that the compound-choking criterion $\beta = 0$, with β as expressed in Eq. (18), is not rigorously correct if one considers non-isentropic flows. It can be found that lifting the hypothesis of isentropic flow leads to the addition of two terms to the expression of β:

$$\beta = p\sum_{i=1}^{n}\frac{A_i}{\rho_i V_i^2}\left(1-M_i^2\right) - \frac{A_i}{\rho_i}\left|\frac{\partial\rho_i}{\partial s_i}\right._p\frac{ds_i}{dp_i} + F_i \tag{19}$$

where F_i comes from the friction term in the momentum conservation equation. As said before, one will here focus on isentropic flows, therefore Eq. (18) will be used as the compound-choking criterion. One now proposes to review the solving algorithm that allows to compute the ejector performance using the compound-choking criterion. Fig. 2 shows the ejector schematic with the notations that are used in the following paragraphs.

The first step is to compute the flow properties through the primary nozzle. In the particular case of isentropic expansions, the primary mass flow rate can be found by imposing Mach unity at the throat. The flow properties at the nozzle exit (section e) can be deduced from conservation of mass, momentum and total enthalpy. Then, the value of the mixing pressure p_y is guessed, as it is impossible to derive the solution in a straightforward manner like when using the Fabri-choking criterion:

$$p_{p,y} = p_{s,y} = p_y = p_{guess} \tag{20}$$

The primary flow properties at section y are found by further expanding the flow until reaching p_y (i.e. using mass, momentum and total enthalpy conservation equations). The secondary flow properties are computed in a similar way, but expanding the flow from the secondary stagnation conditions. First, the enthalpy is computed:

$$h_{s,y} = h\left(p_{s,y}, s_{s,0}\right) \tag{21}$$

The thermodynamic state being defined at section y, the secondary flow density and velocity can be obtained, respectively, as:

$$\rho_{s,y} = \rho\left(p_{s,y}, h_{s,y}\right) \tag{22}$$

$$V_{s,y} = \sqrt{2\left(h_{s,0} - h_{s,y}\right)} \tag{23}$$

The Mach numbers of both streams can then be deduced from their velocities and state at section y. Substituting all quantities previously computed into Eq. (18) gives the expression of the compound-flow indicator for simplified (1D) ejectors:

$$\beta = p_y\left(\frac{A_{p,y}}{\rho_{p,y}V_{p,y}^2}\left(1-M_{p,y}^2\right) + \frac{A_{s,y}}{\rho_{s,y}V_{s,y}^2}\left(1-M_{s,y}^2\right)\right) \tag{24}$$

where the secondary flow area at section y was deduced using the fact that the mixing section is located into the constant (known) area section. One then iterates on the mixing pressure p_y until satisfying the compound-choking criterion. Then, properties at section y are known, and the secondary mass flow rate is computed by:

$$\dot{m}_s = \rho_{s,y}V_{s,y}A_{s,y}, \tag{25}$$

which allows to determine the on-design entrainment ratio ω. To sum up, the difference between the Fabri- and compound choking models comes down to the choice of the mixing pressure p_y. The compound-choking models uses Eq. (24) to fix this pressure value, rather than imposing it to force $M = 1$ for the secondary flow.

4. Results

The results of the RANS model are presented first. These focus on the profiles of the sonic line and the β parameter through the ejector for the operating conditions listed in Table 3. Then, the thermodynamic model accuracy using both the compound-choking and Fabri-choking approaches is showed using the experimental data of [4] as reference.

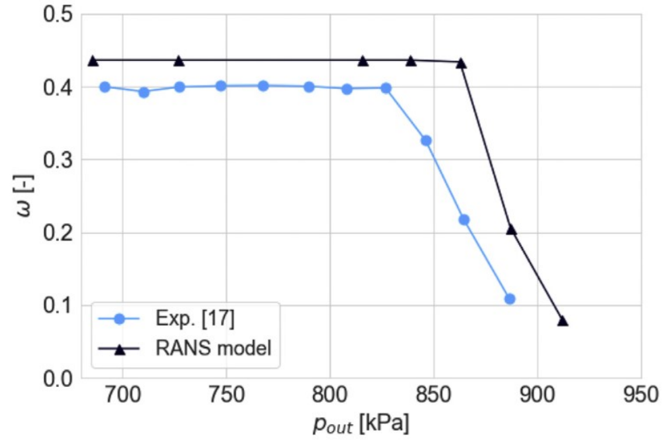

(a)

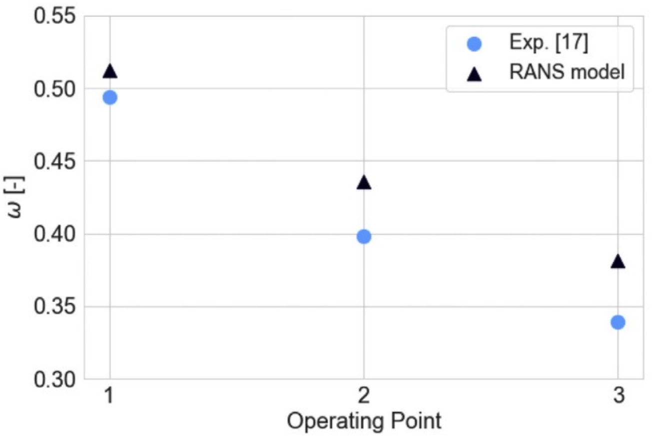

(b)

Fig. 3. Comparison between the numerical results obtained using the RANS model and the experimental data of [17]. (a) ejector operating curve for inlet conditions OP2. (b) double-choke entrainment ratio for inlet conditions OP1 ($T_{p,0}$ = 94.35°C, $p_{p,0}$ = 2888.8 kPa), OP2 ($T_{p,0}$ = 99.15°C, $p_{p,0}$ = 3188.1 kPa) and OP3 ($T_{p,0}$ = 99.15°C, $p_{p,0}$ = 3188.1 kPa). $T_{s,0}$ = 20.05°C and $p_{s,0}$ = 414.6 kPa in all cases.

4.1. RANS model

4.1.1. Experimental validation

The RANS model is validated by comparing its results with the experimental data of [17] for a gas supersonic ejector working with R134a. The ejector geometry is described in Fig. 2 and Table 1. Fig. 3(a) shows the ejector operating curve for the inlet conditions OP2 ($T_{p,0}$ = 94.35°C, $p_{p,0}$ = 2888.8 kPa, $T_{s,0}$ = 20.05°C and $p_{s,0}$ = 414.6 kPa). In terms of the double-choke entrainment ratio, the experimental deviation is about 9% ($\omega_{exp} = 0.398$ vs. ω_{RANS} = 0.436). In terms of the limiting pressure, the deviation is about 4% ($p_{lim,exp}$ = 826.6 kPa vs. $p_{lim,RANS}$ = 862.6 kPa). Moreover, Fig. 3(b) compares the double choke entrainment ratio for three different operating conditions: OP1 ($T_{p,0}$ = 89.35°C, $p_{p,0}$ = 2598.0 kPa), OP2 ($T_{p,0}$ = 94.35°C, $p_{p,0}$ = 2888.8 kPa) and OP3 ($T_{p,0}$ = 99.15°C, $p_{p,0}$ = 3188.1 kPa). For all conditions $T_{s,0}$ = 20.05°C and $p_{s,0}$ = 414.6 kPa. The experimental deviation goes from 4% at OP1 to 12% at OP3. These results show the capacity of the model to capture both the double-choke entrainment ratio and the limiting pressure for various conditions. Although the validation has been carried out solely for R134a, a similar model performance can be expected for the HFOs, given that they remain in the gas phase through the device and they are designed to behave similarly to R134a.

4.1.2. Pure R134a

This section presents the results for the ejector using R134a at conditions OP1. First, the general flow structure through the ejector for the three operating regimes (on-design, critical point and off-design) is shown in Fig. 4 using contours of static pressure and density gradient magnitude (pseudo-Schlieren). Darker areas indicate a stronger density change. The red iso-lines denote the sonic line with $M = 1$. The region between the sonic line and the ejector axis has $M > 1$. Moreover, the dividing streamline, *i.e.* the boundary between the primary and secondary flows is drawn in black. This line is constructed by tracing a velocity streamline from the primary nozzle lip. The operating points in Fig. 4(a), (b) and (c) correspond to the points *ii*, *iii* and *iv* in Fig. 5. Regarding the on-design or double-choking regime (Fig. 4(a)), the flow through the ejector is characterized by a supersonic confined jet leaving the primary nozzle, which entrains the secondary flow into the constant area section. Both flows remain parallel through this region, where shear interactions are the main energy transfer mechanism. A shock train appears towards the end of the constant area section. The subsonic mixture is further compressed in the diffuser. The shock train is conformed by a series of alternating high and low pressure zones, as well as an increase in the density gradient. Similarly, the darker oblique lines in the primary nozzle exit indicate the appearance of shock cells at the jet core. The jet structure does not change with the outlet pressure which shows that the primary jet remains supersonic for the three assessed conditions. On the other hand, the shock train onset position moves closer to the primary nozzle as the outlet to secondary pressure ratio increases. This is clear when comparing Fig. 4(a) and (b), where the latter corresponds to the maximum pressure ratio before entering the single-choking regime. This point would be the optimal operating condition for the ejector. Note that at both points (Fig. 4(a) and (b)), the sonic line reaches the ejector walls and both primary and secondary flows are supersonic before the shock train onset. A further increase in the compression ratio drives the ejector into the single-choking condition (off-design). At this point, the energy available in the primary jet is not high enough to compress the secondary flow to the desired output value unless the secondary mass flow rate is reduced as it can be seen in Fig. 5. In this case, the flow is characterized by the rapid deceleration of the primary jet and the lack of a shock train in the constant area section. Furthermore, the sonic line does not reach the secondary flow (it does not cross the dividing streamline), which indicates that the secondary flow remains subsonic throughout the ejector.

Fig. 5(a) shows the classical ejector operating curve obtained numerically for the ejector working with *R134a* at the inlet conditions of point OP1 in Table 3. This curve is characterized by two regimes: the on-design (double-choking) regime, where the entrainment ratio is constant; and the off-design (single-choking) regime, where the entrainment ratio decays with the increasing outlet pressure. At on-design conditions, the ejector entrains the maximum secondary flow rate possible and reaches the maximum compression ratio at the limit pressure p_{lim}, i.e., the outlet pressure, which marks the start of the off-design regime. The ejector performance declines as the outlet pressure is increased beyond p_{lim}. The limit between the on-design (constant ω) and off-design (decaying ω) regions is also known as the critical point.

Along the on-design regime, the primary and secondary flows are both choked. As a result, the information cannot propagate upstream and changes in the outlet pressure do not affect the flow

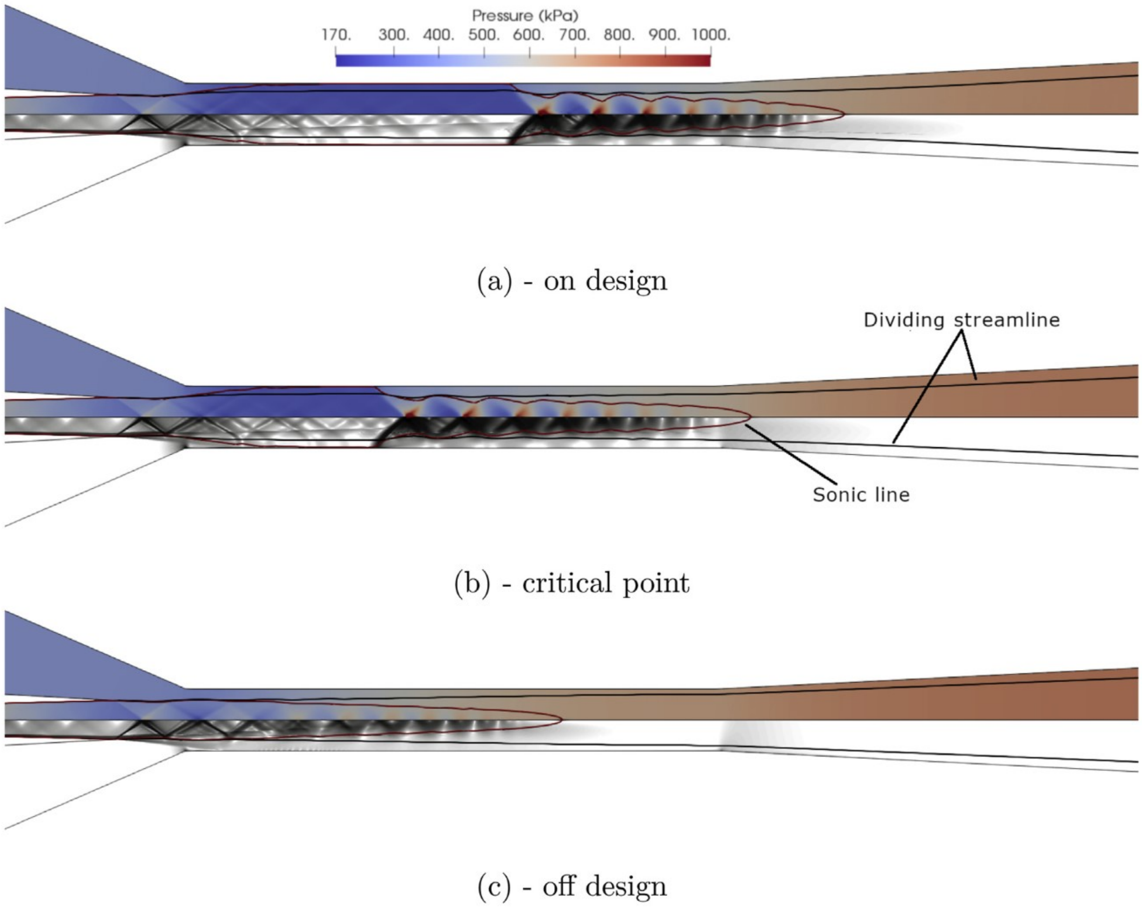

Fig. 4. Static pressure (top) and magnitude of the density gradient $\nabla\rho$ (bottom) contours through the constant area section and the first half of the diffuser for the supersonic ejector working with $R134a$ at inlet conditions OP1 and varying outlet pressure: (a) $p_{out} = 757.2$ kPa (on design condition), (b) $p_{out} = 787.2$ kPa (critical point) and (c) $p_{out} = 807.2$ kPa (off design). Darker areas indicate a higher density gradient. The thin red line is the sonic line or iso-$M = 1$. The thin black line is the dividing streamline. (For interpretation of the references to color in this figure legend, the reader is referred to the Web version of this article.)

at the secondary inlet. Conversely, along the off-design regime, the secondary flow is not choked and any increase in the outlet pressure reduces the secondary mass flow rate. Regarding Fig. 5(a), the critical point may be approximated by extending the black lines, which were produced by fitting a linear regression for the two regimes separately. In general, the secondary flow is considered choked when the local sonic line (the isoline $M = 1$) gets very close to the constant area section walls (because there is still a subsonic section of the boundary layer if the mesh is well resolved at walls). Thus, the limiting pressure p_{lim} would be the value beyond which a further increase in the outlet pressure leads to the detachment of the sonic line. This point is of major interest in ejector design and operation as it maximizes both the entrainment and compression ratios.

Bernstein et al. [13] showed that for parallel gas flows at near sonic conditions, the pressure waves are not able to travel upstream even if some of the individual streams satisfy $M < 1$. This leads to a global mass flow rate independent of the outlet pressure conditions (i.e. a compound-choked flow). In the present study, this theory has been extended to the supersonic ejector assuming real gas conditions as an alternative criterion to predict the choking condition. The local sonic line and the compound-choking indicator (β, Eq. (6)) of four conditions around the critical point for inlet conditions OP1 are shown in Fig. 5(b) and (c), respectively. The curve colors correspond to the points marked in Fig. 5(a).

In Fig. 5(b), the sonic line for the three on-design conditions (points *i-iii*) reaches the ejector wall, which confirms that along the on-design regime, the secondary flow is choked. It can be observed that as conditions approach the critical point, the secondary flow chokes earlier in the mixing duct. Moreover, at the off-design condition (*iv*), the secondary flow is not choked. The compound-choking criterion agrees with the sonic line in this case (Fig. 5(c)). The compound-choking indicator shows that for all on-design conditions, the secondary flow is choked ($\beta \leq 0$). However, when compared to the local sonic line, the choking location is different. The β indicator predicts that the flow chokes at the beginning of the mixing duct ($X/L = 0$) whatever the case. In this study, one considers as choking point the first time the compound-choking indicator crosses down the threshold $\beta = 0$. Further intersections with $\beta = 0$ are due the transition back to a subsonic regime involved by the shock train. In this case, both criteria give the same predictions on the on-design and off-design regimes, but the choking locations are different. According to the β curves, it is worth to mention that the critical point is rather reached for a condition between (*iv*) and (*iii*), where a curve being tangent to $\beta = 0$ should exist at the same location close to $X/L = 0$.

Fig. 6(a) shows the operating curve for the ejector working with $R134a$ at conditions OP2 (Table 3). The corresponding local sonic line and β indicator are displayed in Fig. 6(b) and (c), respectively. Even thought point *vii*, marked by the red dot in Fig. 6(a), sits on the on-design region, the corresponding sonic line in Fig. 6(b) does not reach the ejector wall. The secondary flow is not sonic and a lower

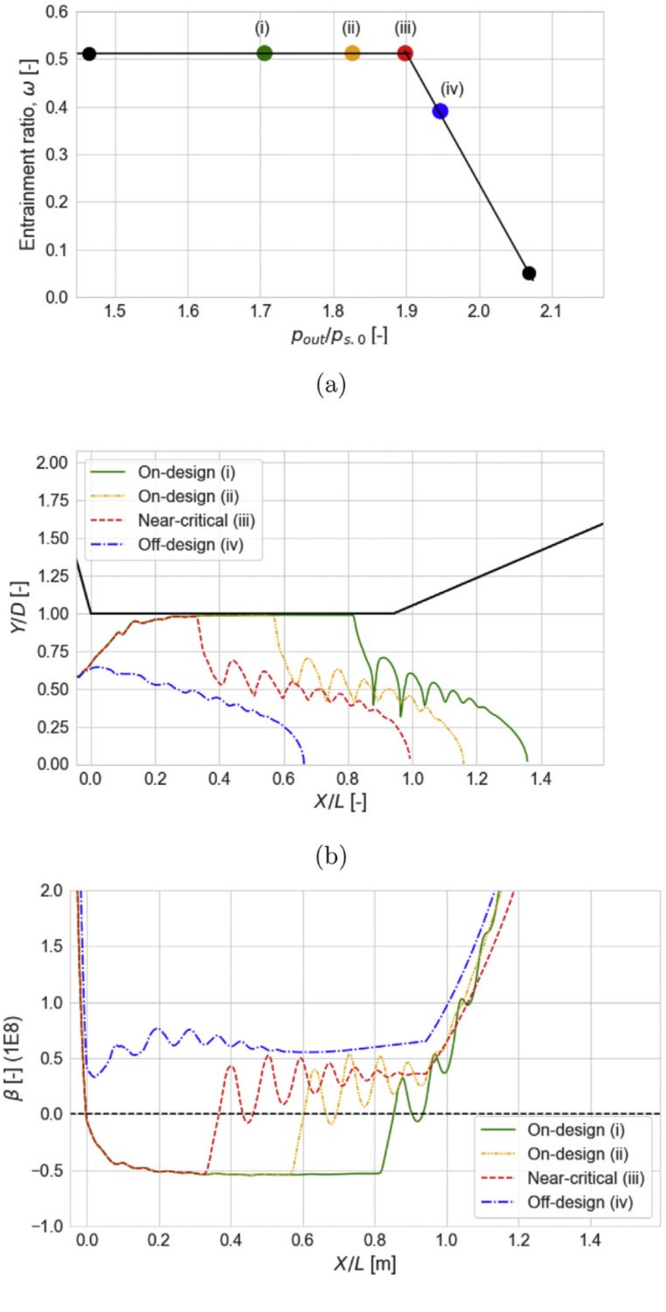

Fig. 5. (a) Operating curve, (b) sonic lines ($Ma = 1$) and (c) compound-choking indicators (β) for the supersonic ejector working with R134a at inlet conditions OP1.

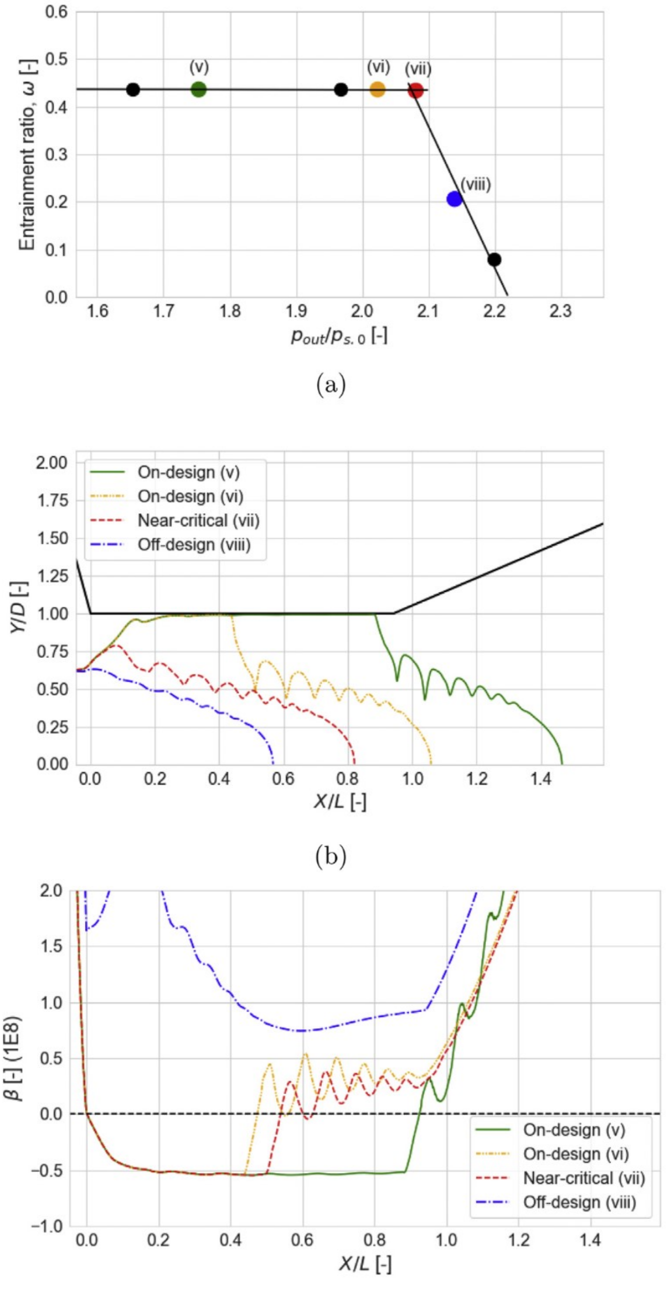

Fig. 6. (a) Operating curve, (b) sonic lines ($Ma = 1$) and (c) compound-choking indicators (β) through the ejector working with R134a at inlet conditions OP2.

entrainment ratio relative to point *vi* should be expected according to this criterion. Thus, the sonic line criterion does not match the observed flow physics. On the other hand, the compound-choking indicator shows that all on-design conditions have a choked secondary flow including point *vii*. Again, the β curves shows that the effective critical point is at a back-pressure between case *vii* and case *vii*.

4.1.3. R134a-HFO mixtures

In this section the influence of the working refrigerant is investigated. Firstly, the original working fluid R134a has been replaced by a mixture of R134a and R1234yf. The operating curve for a mixture of 20% R134a and 80% R1234yf at conditions OP1 along with the corresponding sonic lines and β indicator are displayed in Fig. 7. The global behavior of the ejector with the R134a-R1234yf mixture at these conditions shows a slight decrease of the entrainment ratio (− 3%) and practically the same limiting pressure (+ 1%). Referring to the sonic line for point *xi* (Fig. 7(b)), although it is very close to the ejector wall, it indicates that the secondary flow is not entirely sonic. Yet, the ejector still provides a maximum entrainment ratio at this condition according to Fig. 7(a). Once again, the compound-choking indicator (Fig. 7(c)) agrees better with the ejector performance curve, i.e., a portion of the flow is subsonic but the whole flow is compound-choked. Moreover, it is

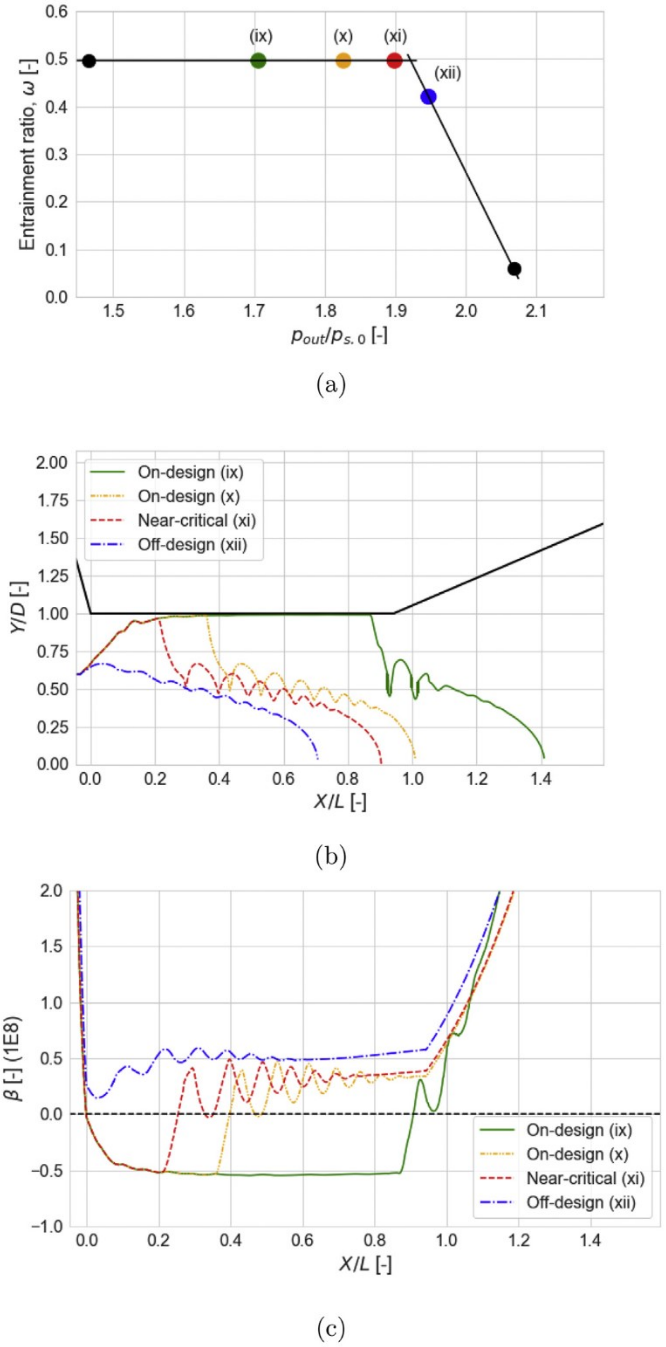

Fig. 7. (a) Operating curve, (b) sonic lines ($Ma = 1$) and (c) compound-choking indicators (β) through the ejector working with a mixture of 20% R134a and 80% R1234yf at inlet conditions OP1.

also shown that the condition *xii* is close of the critical conditions in terms of back-pressure as the blue curve Fig. 7(c) almost comes to the threshold $\beta = 0$.

Regarding the β parameter (Figs. 5(c), 6(c) and 7(c)), the curves corresponding to the on-design cases are superimposed and mark the choking point ($\beta = 0$) at the same location. This remarks that for double-choking conditions, the flow is compound-choked at the same position nearby the beginning of the constant area section. On the other hand, the return to compound-subsonic flow varies with the outlet pressure such that the higher p_{out}, the earlier the transition point. This agrees with the fact that the shock onset location also moves closer to the primary jet as the compression ratio increases. Different from on-design cases, the off-design curves for β are not superimposed with the others and do not cross towards $\beta < 0$, which indicates that the flow remains compound-subsonic through the ejector.

Fig. 8 shows the operating curve, sonic lines and β indicator for the mixture of 20% R134a and 80% R1234ze(E) at OP1. The HFO change in the mixture leads to a decrease of the entrainment ratio, from 0.496 to 0.408. However, the maximum compression ratio augments from 1.92 to 2.07. In this case, both the sonic line and the

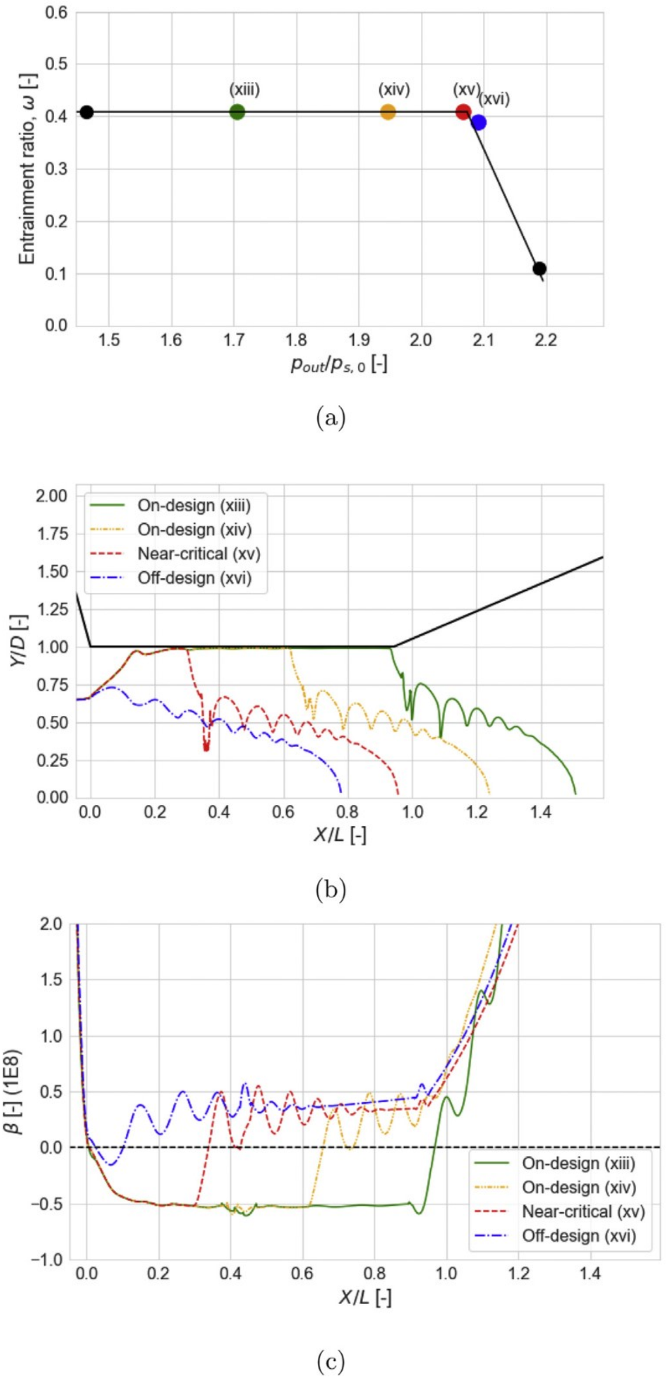

Fig. 8. (a) Operating curve, (b) sonic lines ($Ma = 1$) and (c) compound-choking indicators (β) through the ejector working with a mixture of 20% R134a and 80% R1234ze(E) at inlet conditions OP1.

compound-choking criterion agree on the determination of the on-design and off-design points. For the latter condition, point *xvi*, the β parameter crosses the threshold $\beta = 0$ at $X/L = 0.02$ m and goes again above $\beta = 0$ at $X/L = 0.1$. This case is very close to the limit case where $\beta = 0$ would be reached by a tangent point on Fig. 8(c). Theoretically, this situation is the limit case of the compound-choking condition. However, it is clear the total ejector flow rate is not maximum any more but starts decreasing as illustrated by point *xvi* in Fig. 8(a). In this limit case, the wrong physical interpretation of the β value comes from the fact that the isentropic assumption of the model becomes less verified in the region when the predicted choking is strongly affected by a shock-train. This is not the case for the other conditions where β goes well under the negative values before going back to be positive when the shock-train occurs.

Moreover, Fig. 9(a), (b) and (c) illustrate, respectively, the operating curve, sonic lines and β indicator for the ejector using an 80% R134a-20% R1234yf mixture at conditions OP2. In comparison with the results obtained for pure R134a, the global performance of the ejector is almost identical. This is expected given the very high percentage of R134a in the mixture. A particularity in this case is that the compound-choking indicator for the off-design condition (point *xx*) barely reaches $\beta = 0$ before returning to the compound-subsonic regime at the beginning of the mixing duct. This can be regarded as the limit case previously mentioned. Although the compound-choking theory would lead to claim a compound-choked condition, and then a maximum entrainment, the fact that this occurs in the stronger non-isentropic area of the shock train, leads to a wrong interpretation of the physics. Indeed, at this condition, the entrainment is not maximum (Fig. 9(a)).

Using the compound flow theory [15], predicted the entrainment ratio of supersonic ejectors with a better accuracy than the base model of [4], assuming ideal gas and isentropic behaviour. The results presented here show that this theory can be extended to accommodate real gases. It also verifies that it offers a more physically-sound explanation of the choking process, and a more accurate way to determine the operating regime of the ejector than the Fabri-choking based methods. The RANS results confirm that the flow is compound-choked (and hence the ejector is in the double-choking regime) when the β parameter clearly crosses the $\beta = 0$ threshold and remain smoothly in negative values. When the β curve crosses the threshold in a flow area affected by non-isentropic conditions, such as in the occurrence of a shock-train, the limits of the model are reached and this could give wrong interpretation on the choking conditions.

4.2. Thermodynamic model

Results provided by both models (Fabri and compound) are compared to the 39 experimental cases of Huang et *al.* [4] for R141b in Tables 4 and 5. The associated graphs of error are presented in Fig. 10(a) and (b) for the Fabri-choking and the compound-choking, respectively. The relative error is defined as:

$$\text{Error} = \frac{\omega_{mod} - \omega_{exp}}{\omega_{exp}} \tag{26}$$

with ω_{exp} and ω_{mod} the entrainment ratios obtained from the experiments and the model, respectively. As can be seen, the model provides quite poor results using the Fabri-choking criterion, with relative errors that can reach values up to 53.09% (for case 10) and a mean error of 17.54%. It also appears very clearly that the model tends to underestimate the entrainment ratio, with most predictions having a deviation of maximum 20% (Fig. 10(a)). The results provided by the compound-choking theory are much better than

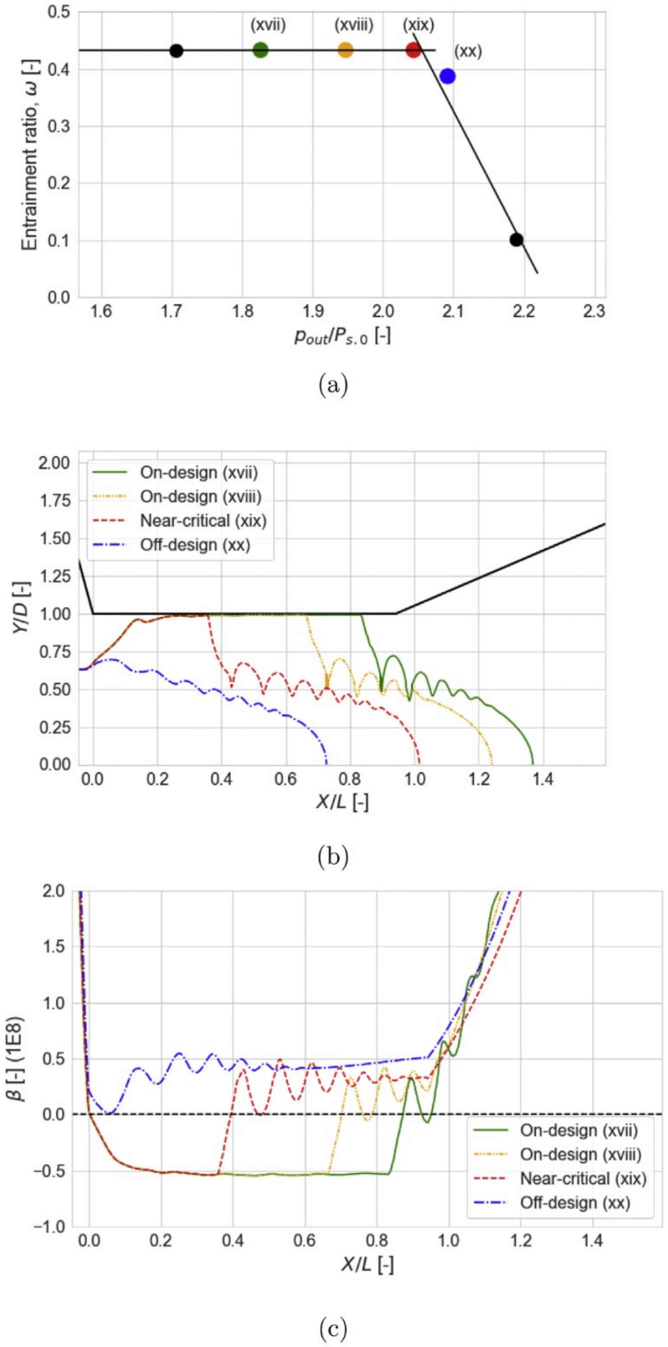

Fig. 9. (a) Operating curve, (b) sonic lines ($Ma = 1$) and (c) compound-choking indicators (β) through the ejector working with a mixture of 80% R134a and 20% R1234yf at inlet conditions OP2.

those predicted by the Fabri-choking theory. One may observe that the better part of the predictions lie within a 10% error from the experimental data (Fig. 10(b)), with a mean error of 5.28%. The compound-choking criterion also tends to underestimate the entrainment ratio, but to a lesser extent. This slight underestimation is however positive from a design perspective, as it is conservative. The fact that both models tend to underestimate the entrainment ratio is likely explained by the restrictive assumption that the mixing pressure p_y is constant along section *y*. Indeed, the fact that the secondary pressure has to match the primary pressure may hinder the predicted secondary mass flow rate, as complex

Table 4
Predictions of the entrainment ratio for the ejector configurations of Huang et al.[4] using the Fabri-choking and the compound-choking criteria (cases 1–25).

Case	Ejector	A_y/A_t	$p_{p,0}$ [bar] (T_{sat}[$^\circ C$])	$p_{s,0}$ [bar] (T_{sat}[$^\circ C$])	ω (exp)	ω (Fabri)	Error [%] (Fabri)	ω (CPC)	Error [%] (CPC)
1	EH	10.64	6.04 (95)	0.4 (8)	0.4377	0.3957	−9.60	0.4302	−1.71
2	EF	9.83	6.04 (95)	0.4 (8)	0.3937	0.3362	−14.61	0.3737	−5.08
3	AD	9.41	6.04 (95)	0.4 (8)	0.3457	0.3054	−11.66	0.3446	−0.32
4	EE	9.17	6.04 (95)	0.4 (8)	0.3505	0.2877	−17.92	0.3281	−6.39
5	AC	8.28	6.04 (95)	0.4 (8)	0.2814	0.2223	−21.00	0.2674	−4.98
6	ED	8.25	6.04 (95)	0.4 (8)	0.2902	0.2201	−24.16	0.2654	−8.55
7	EC	7.26	6.04 (95)	0.4 (8)	0.2273	0.1474	−35.15	0.1994	−12.27
8	AG	7.73	6.04 (95)	0.4 (8)	0.2552	0.1819	−28.72	0.2305	−9.68
9	EG	6.77	6.04 (95)	0.4 (8)	0.2043	0.1114	−45.47	0.1676	−17.96
10	AA	6.44	6.04 (95)	0.4 (8)	0.1859	0.0872	−53.09	0.1466	−21.14
11	AD	9.41	5.38 (90)	0.4 (8)	0.4446	0.3797	−14.60	0.4156	−6.52
12	AC	8.28	5.38 (90)	0.4 (8)	0.3488	0.3797	−10.47	0.328	−5.96
13	AG	7.73	5.38 (90)	0.4 (8)	0.304	0.3276	−15.63	0.286	−5.92
14	AB	6.99	5.38 (90)	0.4 (8)	0.2718	0.2577	−17.32	0.2304	−15.23
15	AA	6.44	5.38 (90)	0.4 (8)	0.2246	0.2057	−28.58	0.1898	−15.49
16	AD	9.41	4.65 (84)	0.4 (8)	0.5387	0.4865	−9.69	0.5186	−3.73
17	AC	8.28	4.65 (84)	0.4 (8)	0.4241	0.3797	−10.47	0.4164	−1.82
18	AG	7.73	4.65 (84)	0.4 (8)	0.3883	0.3276	−15.63	0.3672	−5.43
19	AB	6.99	4.65 (84)	0.4 (8)	0.3117	0.2577	−17.32	0.3018	−3.18
20	AA	6.44	4.65 (84)	0.4 (8)	0.288	0.2057	−28.58	0.254	−11.81
21	AD	9.41	4.00 (78)	0.4 (8)	0.6227	0.6142	−1.37	0.6428	3.23
22	AC	8.28	4.00 (78)	0.4 (8)	0.4889	0.4907	0.37	0.5234	7.06
23	AG	7.73	4.00 (78)	0.4 (8)	0.4393	0.4306	−1.98	0.4658	6.03
24	AB	6.99	4.00 (78)	0.4 (8)	0.3922	0.3497	−10.84	0.3889	−0.84
25	AA	6.44	4.00 (78)	0.4 (8)	0.3257	0.2895	−11.11	0.3325	2.09

Table 5
Predictions of the entrainment ratio for the ejector configurations of Huang et al.[4] using the Fabri-choking and the compound-choking criteria (cases 26–39).

Case	Ejector	A_y/A_t	$p_{p,0}$ [bar] (T_{sat}[$^\circ C$])	$p_{s,0}$ [bar] (T_{sat}[$^\circ C$])	ω (exp)	ω (Fabri)	Error [%] (Fabri)	ω (CPC)	Error [%] (CPC)
26	EF	9.83	6.04 (95)	0.47 (12)	0.4989	0.4456	−10.68	0.479	−3.99
27	EE	9.17	6.04 (95)	0.47 (12)	0.4048	0.3889	−3.93	0.4249	4.97
28	AD	9.41	6.04 (95)	0.47 (12)	0.4541	0.4095	−9.82	0.4445	−2.11
29	AG	7.73	6.04 (95)	0.47 (12)	0.3503	0.2654	−24.24	0.3085	−11.93
30	EC	7.26	6.04 (95)	0.47 (12)	0.304	0.2251	−25.95	0.2712	−10.79
31	AA	6.44	6.04 (95)	0.47 (12)	0.235	0.1547	−34.17	0.2073	−11.79
32	AD	9.41	5.38 (90)	0.47 (12)	0.5422	0.497	−8.34	0.529	−2.43
33	AG	7.73	5.38 (90)	0.47 (12)	0.4034	0.3359	−16.73	0.3752	−6.99
34	AA	6.44	5.38 (90)	0.47 (12)	0.2946	0.2121	−28.00	0.2601	−11.71
35	AD	9.41	4.65 (84)	0.47 (12)	0.635	0.6226	−1.95	0.6512	2.55
36	AG	7.73	4.65 (84)	0.47 (12)	0.479	0.4371	−8.75	0.4723	−1.40
37	AA	6.44	4.65 (84)	0.47 (12)	0.3398	0.2946	−13.30	0.3375	−0.68
38	AD	9.41	4.00 (78)	0.47 (12)	0.7412	0.7727	4.25	0.7981	7.68
39	AG	7.73	4.00 (78)	0.47 (12)	0.6132	0.5582	−8.97	0.5895	−3.86

fluid structures are produced in a real ejector [28].

5. Conclusions

This study showed the feasibility of using the compound-choking theory of Bernstein et al. [13] for determining the critical operating point of supersonic gas ejectors assuming real gas properties. This theory has been first extended analytically to real gas refrigerants. Then, the different behaviors of the Fabri-choking criterion (sonic line criterion) and the β parameter proposed by the compound-choking theory were compared using a Wall-resolved RANS model for different refrigerant mixtures and operating conditions. Secondly, a thermodynamic model for the prediction of the double-choking entrainment ratio has been developed and compared with a similar model proposed by Chen et al. [8] (based on the Fabri-choking criterion). Based on the results discussed above, the following conclusions are drawn:

- Within the range of operating conditions and refrigerants assessed with the RANS model, using the β criterion profile through the ejector is a more definite way for determining the operating regime than the sonic line criterion, especially close to the critical point.
- Close to the critical operating point, a double-choking entrainment ratio can be attained even if the secondary flow is not entirely sonic according to the sonic line profile, demonstrating the compound-choking physics is more general then the simpler Fabri phenomenology, which a particular case
- By using the compound-choking theory in a 1D model, the double-choking entrainment ratio can be predicted with a mean error of 5.28% (with most predictions lying within 10% of the experimental data). In contrast, the Fabri-choking approach results in a mean error of 17.54%. There is virtually no difference on the complexity or the computational cost of using one approach over the other. It paves the way towards the

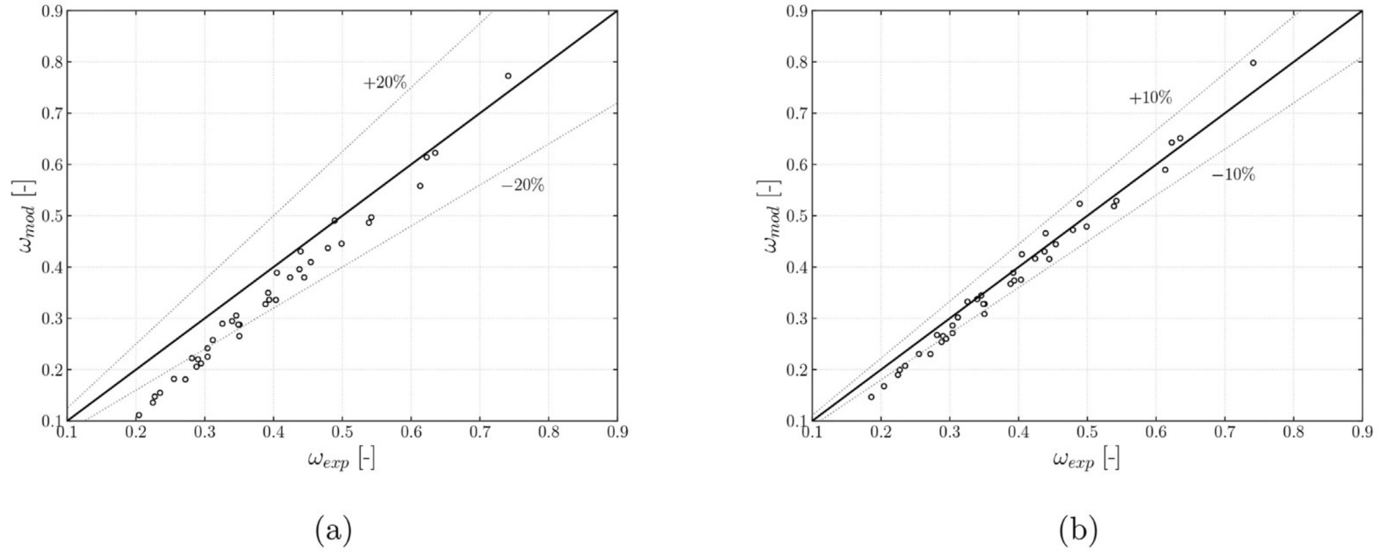

Fig. 10. Comparisons in terms of the entrainment ratio between the thermodynamic model based on (a) the Fabri-choking and (b) the compound choking criterion and the experimental data of [4] for supersonic ejectors working with R141b.

development of more accurate thermodynamic models for the design of future ejector-based refrigeration cycles.

In a close future, this compound-choking criterion needs to be extended to two-phase ejector flows, in particular using carbon dioxide as refrigerant. Nowadays, transcritical CO_2 ejector-based systems are indeed very popular when associated to cooling cycles.

Declaration of competing interest

The authors declare that they have no known competing financial interests or personal relationships that could have appeared to influence the work reported in this paper.

Acknowledgments

The authors acknowledge the support of the NSERC chair on industrial energy efficiency established in 2019 at Université de Sherbrooke funded by Hydro-Québec, Natural Resources Canada (CanmetEnergy-Varennes) and Emerson Canada. Computational resources have been provided by Compute Canada.

Signs and symbols

Acronyms

CFD	Computational fluid dynamics
COP	Coefficient of performance [−]
CPC	Compound-choking criteria
CSA	Constant section area
HDRC	Heat driven refrigeration cycle
HFO	Hydrofluoroolefin
OP1, OP2	Operating points 1 and 2

Math symbols

$A(x)$	Cross-sectional area at position X [m2]
$A(i)$	i-th sub-stream cross-sectional area [m2]
c	Speed of sound [ms^{-1}]
d	Primary nozzle exit diameter [mm]
D	Mixing chamber diameter [mm]
e_d	Outlet diameter [mm]
F	Friction term [−]
G	Mass flowrate per unit area [kg m^{-2} s^{-1}]
h	Specific enthalpy [kJ kg^{-1}]
l	Mixing chamber length [mm]
L	Diffuser length [mm]
M	Mach number [−]
$\dot{m}$	Mass flowrate [kg s^{-1}]
n_d	Primary nozzle throat diameter [mm]
NXP	Nozzle exit position [mm]
p_{lim}	Limiting outlet pressure [kPa]
$p_{0,i}$	i-th sub-stream inlet pressure [kPa]
p	Pressure [kPa]
Rg	Perfect gas constant [kJ K^{-1} kg^{-1}]
s	Specific entropy [kJ $kg^{-1}K^{-1}$]
T	Temperature [°C]
$T_{0,i}$	i-th sub-stream inlet temperature [°C]
V	Velocity [ms^{-1}]
X	Horizontal coordinate [meter]
y^+	Dimensionless wall coordinate [−]
Y	Radial coordinate [meter]

Greek characters

α	Speed of the compound wave [ms^{-1}]
β	Compound-flow indicator [−]
γ	Heat capacity ratio [−]
Γ	Ejector compression ratio [−]
ρ	Density [kg m^{-3}]
ω	Ejector entrainment ratio [−]

Subscripts

0	inlet condition
exp	Experimental value
i	*i*-th sub-stream
mod	Model (predicted) value
RANS	RANS (predicted) value
out	Condition at outlet
p	Primary stream
s	Secondary stream

y Condition at cross-section *y*

References

[1] Aidoun Z, Ameur K, Falsafioon M, Badache M. Current advances in ejector modeling, experimentation and applications for refrigeration and heat pumps. Part 1: single-phase ejectors. Inventions 2019;4(1):15.
[2] Grazzini G, Milazzo A, Mazzelli F. Ejectors for efficient refrigeration: design, applications and computational fluid dynamics. Elsevier; 2018.
[3] Chou S, Yang P, Yap C. Maximum mass flow ratio due to secondary flow choking in an ejector refrigeration system. Int J Refrig 2001;24(6):486–99.
[4] Huang B, Chang J, Wang C, Petrenko V. A 1-D analysis of ejector performance. Int J Refrig 1999;22(5):354–64.
[5] Zhu Y, Cai W, Wen C, Li Y. Shock circle model for ejector performance evaluation. Energy Convers Manag 2007;48(9):2533–41.
[6] Garcia del Valle J, Jabardo J, Ruiz F, Alonso J. A one dimensional model for the determination of an ejector entrainment ratio. Int J Refrig 2012;35(4):772–84.
[7] Chen W, Liu M, Chong D, Yan J, Little A, Bartosiewicz Y. A 1D model to predict ejector performance at critical and sub-critical operational regimes. Int J Refrig 2013;36(6):1750–61.
[8] Chen W, Shi C, Zhang S, Chen H, Chong D, Yan J. Theoretical analysis of ejector refrigeration system performance under overall modes. Appl Energy 2017;185:2074–84.
[9] Ma Z, Bao H, Roskilly A. Thermodynamic modelling and parameter determination of ejector for ejection refrigeration systems. Int J Refrig 2017;75:117–28.
[10] Croquer S, Poncet S, Aidoun Z. Thermodynamic modeling of supersonic gas ejector with droplets. Entropy 2017;19(579):1–21.
[11] Fabri J, Siestrunck R. Supersonic air ejectors. Adv Appl Mech 1958;5:1–34.
[12] Lamberts O, Chatelain P, Bartosiewicz Y. Numerical and experimental evidence of the Fabri-choking in a supersonic ejector. Int J Heat Fluid Flow 2018;69:194–209.
[13] Bernstein A, Heiser WH, Hevenor C. Compound-compressible nozzle flow. J Appl Mech 1967;34:548–54.
[14] Pearson H, Hollyday J, Smith S. A theory of the cylindrical ejector supersonic propelling nozzle. Journal of the Royal Aeronautical Society 1958;62(574):746751.
[15] Lamberts O, Chatelain P, Bourgeois N, Bartosiewicz Y. The compound-choking theory as an explanation of the entrainment limitation in supersonic ejectors. Energy 2018;158:524–36.
[16] Croquer S, Poncet S, Aidoun Z. Turbulence modeling of a single-phase R134a supersonic ejector. Part 1: numerical benchmark. Int J Refrig 2016;61:140–52.
[17] Garca del Valle J, Saiz Jabardo J, Castro Ruiz F, San José Alonso J. An experimental investigation of a R134a ejector refrigeration system. Int J Refrig 2014;46:105–13.
[18] Fang Y, Croquer S, Poncet S, Aidoun Z, Bartosiewicz Y. Drop-in replacement in a R134 ejector refrigeration cycle by HFO refrigerants. Int J Refrig 2017;77:87–98.
[19] Yang M, Zhang H, Meng Z, Qin Y. Experimental study on R1234yf/R134a mixture (R513a) as R134a replacement in a domestic refrigerator. Appl Therm Eng 2019;146:540–7.
[20] Mota-Babiloni A, Navarro-Esbrí J, Barragán-Cervera Á, Molés F, Peris B. Experimental study of an R1234ze(E)/R134a mixture (R450a) as R134a replacement. Int J Refrig 2015;51:52–8.
[21] Bartosiewicz Y, Aidoun Z, Desevaux P, Mercadier Y. Numerical and experimental investigations on supersonic ejectors. Int J Heat Fluid Flow 2005;26(1):56–70.
[22] Li C, Li Y. Investigation of entrainment behavior and characteristics of gas-liquid ejectors based on CFD simulation. Chem Eng Sci 2011;66:405–16.
[23] Yazdani M, Alahyari A, Radcliff T. Numerical modeling of two-phase supersonic ejectors for work-recovery applications. Int J Heat Mass Tran 2012;55:5744–53.
[24] Lemmon EW, Bell IH, Huber ML, McLinden MO. NIST standard reference database 23: reference fluid thermodynamic and transport properties-REFPROP. National Institute of Standards and Technology; 2018., Version 10.0. https://www.nist.gov/srd/refprop.
[25] Ayachit U. The Paraview guide: a parallel visualization application. Kitware, Inc.; 2015.
[26] Croquer S, Poncet S, Aidoun Z. Gas supersonic ejector performance with droplet injection: a combined CFD and thermodynamic modelling approach. In: Minea V, editor. Proceedings of the 25th IIR international congress of refrigeration. Montreal, Canada: International Institute of Refrigeration; 2019. p. 1863–70.
[27] Bell IH, Wronski J, Quoilin S, Lemort V. Pure and pseudo-pure fluid thermophysical property evaluation and the open-source thermophysical property library CoolProp. Ind Eng Chem Res 2014;53(6):2498–508.
[28] Croquer S, Lamberts O, Moreau S, Bartosiewicz Y, Poncet S. Modélisation d'un éjecteur supersonique à air: du modèle RANS à la simulation des grandes échelles. In: XIVème Colloque International Franco-Québécois en énergie; 2019. Baie St-Paul, Canada.